Spin-Lattice Relaxation Times of Single Donors and Donor Clusters in Silicon

Yu-Ling Hsueh,[1,*] Holger Büch,[2] Yaohua Tan,[1] Yu Wang,[1] Lloyd C. L. Hollenberg,[3] Gerhard Klimeck,[1] Michelle Y. Simmons,[2] and Rajib Rahman[1,†]

[1]*Network for Computational Nanotechnology, Purdue University, West Lafayette, Indiana 47907, USA*

[2]*Center for Quantum Computation and Communication Technology, School of Physics, University of New South Wales, Sydney, NSW 2052, Australia*

[3]*Center for Quantum Computation and Communication Technology, School of Physics, University of Melbourne, VIC 3010, Australia*

(Received 14 March 2014; revised manuscript received 16 May 2014; published 11 December 2014)

An atomistic method of calculating the spin-lattice relaxation times (T_1) is presented for donors in silicon nanostructures comprising of millions of atoms. The method takes into account the full band structure of silicon including the spin-orbit interaction. The electron-phonon Hamiltonian, and hence, the deformation potential, is directly evaluated from the strain-dependent tight-binding Hamiltonian. The technique is applied to single donors and donor clusters in silicon, and explains the variation of T_1 with the number of donors and electrons, as well as donor locations. Without any adjustable parameters, the relaxation rates in a magnetic field for both systems are found to vary as B^5, in excellent quantitative agreement with experimental measurements. The results also show that by engineering electronic wave functions in nanostructures, T_1 times can be varied by orders of magnitude.

DOI: 10.1103/PhysRevLett.113.246406 PACS numbers: 76.60.Es, 63.20.kd, 71.70.Ej, 85.35.Gv

Because of the extremely long spin coherence times, in some cases, exceeding seconds [1,2], and the existing industrial fabrication infrastructure, silicon is well suited to be an outstanding platform for semiconductor quantum computer technology [3–8]. Qubits hosted by donors in silicon [3] have some added advantages as they are readily available few-electron systems with a rich electronic structure and can form identical qubits [9]. In the last few years, several key experimental milestones have been achieved in dopant based quantum computing, including the demonstration of electron [10] and nuclear [11] spin qubits, single spin readout and initialization [12,13], and the observation of spin blockade and exchange towards two qubit coupling [14,15]. Recent advances in scanning tunneling microscope (STM) lithography has enabled placement of single donors with atomic scale precision [16], with the result that various functional units such as quantum wires [17], single electron transistors (SET) [13,18], and quantum dots [19] can all be realized in plane with densely packed donor islands. The STM approach provides the fabrication precision needed to develop test-bed quantum chips for the demonstration of quantum algorithms in a solid-state quantum computer.

One of the two most important time scales for a spin qubit is the spin-lattice relaxation time (T_1). Recent experiments have measured T_1 times in a single donor and in a few-donor cluster indicating shorter T_1 times in the latter [12,13]. Previous theoretical works exist in the literature qualitatively describing two different spin relaxation mechanisms in a bulk donor system [20,21]. However, a comprehensive quantitative theory which combines all the different mechanisms under a unified framework and accounts for the local inhomogeneous environment of the donors in a realistic nanostructure is still lacking. Moreover, there is no theoretical work yet to explain the measured T_1 times in densely packed donor clusters. In this Letter, we present a comprehensive approach to compute the T_1 times in single donors and donor clusters in silicon nanostructures based on the self-consistent atomistic tight-binding (TB) method. The computed T_1 times can explain the experimental results of Refs [12,13] without any adjustable parameters. The T_1 times are found to depend strongly on the size and shape of the electronic wave functions, which suggests that quantum confinement plays an important role in the relaxation process. The calculations also provide an insight into how the T_1 times can be engineered by several orders of magnitude in these quantum devices.

Single shot measurements of the donor-bound electron spin performed in ion-implanted metal-oxide-semiconductor (MOS) devices yielded a T_1 time of 2.3 s at $B = 2$ T and a B^5 dependency of the relaxation rate ($1/T_1$) [12]. Similar T_1 measurements have since been performed in a STM patterned donor cluster in an all epitaxially engineered device with atomic scale precision, giving T_1 time of 0.4 s at $B = 2$ T and a similar B^5 dependency of the relaxation rate [13]. The donor clusters are composed of several donors with an average separation less than or equal to the single donor Bohr radii [Fig. 1(b)] which can host several electrons. Such a cluster provides for additional addressability within an array of qubits [13]. In general, the T_1 times of donors in realistic devices and nanostructures are likely to be influenced by the inhomogeneous environment and need to be understood from an atomic scale theory.

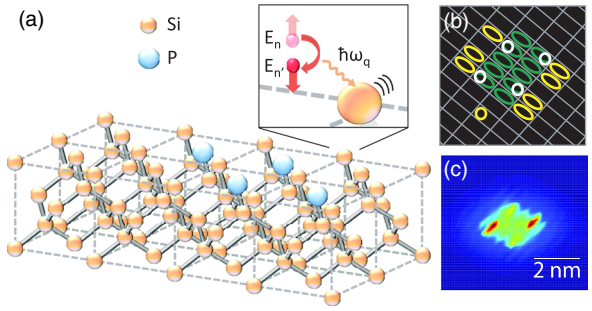

FIG. 1 (color online). (a) Schematic plot of a $4P$ donor cluster in silicon. The cluster hosts an up spin electron with energy E_n which relaxes to the down spin state $E_{n'}$ by emitting a phonon with energy $\hbar\omega_q$. (b) An STM template of a $4P$ cluster showing example dimer locations [13]. (c) The computed self-consistent probability density of the outermost electron in a $4P$ donor cluster with five electrons ($4P5e$).

The full TB Hamiltonian of the silicon and the P atoms was represented with a 20-orbital $sp^3d^5s^*$ basis per atom including nearest-neighbor and spin-orbit interactions [22–24]. A donor was represented by a Coulomb potential of a positive charge screened by the dielectric constant of Si and subjected to an on site cutoff potential [25,26]. The model reproduces the full energy spectrum of a single donor including valley-orbit splitting [27], and also captures the single donor hyperfine [25] and spin-orbit Stark effects [28], in close agreement with experiments. Recent STM imaging of the donor wave function also shows excellent agreement with the tight-binding wave function at the atomic scale [29]. The magnetic field is represented by a vector potential in a symmetric gauge and entered through a Peierls substitution. To capture multielectron occupation of the donor clusters, a self-consistent Hartree method was employed, in which the electronic charge density was computed from the N lowest energy occupied wave functions, $n(r) = \sum_i^N |\Psi_i(r)|^2$. Solving the potential due to $n(r)$ self-consistently with the tight-binding Hamiltonian until convergence enables us to obtain the binding energies and the wave functions of the few electrons bound to the donor cluster. This method has also successfully reproduced the experimental D^- (i.e., the second electron bound to a single P) binding energy [18,30]. Exchange and correlation terms based on local density approximation are added to the Hartree potential [31]. The same methodology has been used to reproduce experimentally measured addition energies of multidonor clusters [15]. The TB Hamiltonian of about 1.4 million atoms including the Hartree potential is then solved by a parallel Block Lanczos algorithm to obtain the relevant lowest energy wave functions.

For the relaxation times computed in this Letter, we assume that an electron has been loaded to the ground state of a single donor or a donor cluster. In case of a bulk P donor, this represents the A_1 state at -45.6 meV below the conduction band [32]. This binding energy can vary with donor depths and fields in a realistic device [27]. In addition, the binding energy in a donor cluster can be sensitive to the donor numbers, electron numbers, and donor locations. Experimentally, the electron can be loaded in the ground state of the donor or cluster by bringing the Fermi level of an electron reservoir in resonance with the Zeeman split ground state, as demonstrated in Refs. [12,13].

The relaxation rate $1/T_1$, for an electron-phonon interaction Hamiltonian $\hat{H}_{ep}$ can be obtained by Fermi's golden rule,

$$\frac{1}{T_1} = \frac{2\pi}{\hbar}|\langle n', n_q + 1|\hat{H}_{ep}|n, n_q\rangle|^2\delta(E_n - E_{n'} - \hbar\omega_q), \quad (1)$$

where n and n' are the up and down spin electronic states with energy E_n and $E_{n'}$, respectively, ω_q is the angular frequency of the emitted phonon, n_q and $n_q + 1$ are the initial and final phonon states with wave vector q. In the B-field range of experimental interest [12,13], the Zeeman splitting is less than 1 meV. As a result, only acoustic phonons contribute to the spin relaxation process. $\hat{H}_{ep}$ then depends on the deformation potential of the crystal $\hat{\Xi}_{ij}$ (i, j representing each of the three Cartesian directions) and the strain tensor components $\hat{U}_{ij}$ [33] (both of which are position dependent in the atomistic TB method), and is given by

$$\hat{H}_{ep} = \sum_{i,j}\hat{\Xi}_{ij}\hat{U}_{ij}. \quad (2)$$

To evaluate $\hat{\Xi}_{ij}$, we use the relation $\hat{\Xi}_{ij} = (\partial\hat{H}_{ep}/\partial\hat{U}_{ij})$, and compute the total change in the electron-phonon Hamiltonian $\Delta\hat{H}_{ep}$ due to an infinitesimal uniform lattice strain represented by $\Delta\hat{U}_{ij} = u_{ij}$ (a small arbitrary constant). Since $\Delta\hat{H}_{ep}$ can be expressed as a change in the electronic TB Hamiltonian $\hat{H}_e$ under a crystal deformation caused by u_{ij} [33,34], $\hat{\Xi}_{ij}$ is given as

$$\hat{\Xi}_{ij} = \{\hat{H}_e(u_{ij}) - \hat{H}_e(0)\}/u_{ij}. \quad (3)$$

The strain dependent TB Hamiltonian $\hat{H}_e(u_{ij})$ expresses the TB matrix elements as functions of interatomic bond lengths and distortion angles depending on the relative positions of pairs of atoms in the lattice [35]. This method of incorporating local strain in the TB Hamiltonian is well established and has been shown to reproduce various experimental results [22]. Although we have considered all six components of $\hat{\Xi}_{ij}$, we have found the off diagonal terms to be small for single donor states located near the conduction band.

Furthermore, $\hat{U}_{ij}$ can also be expressed in terms of phonon creation and annihilation operators, $\hat{a}_q^+$ and $\hat{a}_q$, respectively, as

$$\hat{U}_{\mathrm{ij}} = \frac{1}{2}\sum_{q}\left(\frac{\hbar}{2V\rho\omega_q}\right)^{(1/2)} i(e_{\mathrm{qi}}q_j + e_{\mathrm{qj}}q_i)\{\hat{a}_q^{+}\exp[i(\mathbf{q}\cdot\mathbf{r})] + \hat{a}_q\exp[-i(\mathbf{q}\cdot\mathbf{r})]\}, \quad (4)$$

where V is the volume of the crystal, ρ the mass density, and $\mathbf{e_q}$ the phonon polarization unit vector. Using Eqs. 2 and 4, the matrix element of $\hat{H}_{ep}$ can be expressed as,

$$\langle n', n_q + 1|\hat{H}_{ep}|n, n_q\rangle = \frac{1}{2}\sum_{q}\left(\frac{\hbar}{2V\rho\omega_q}\right)^{(1/2)}\sqrt{n_q+1} \times \sum_{i,j} i(e_{\mathrm{qi}}q_j + e_{\mathrm{qj}}q_i)\langle n'|\exp[i(\mathbf{q}\cdot\mathbf{r})]\hat{\Xi}_{\mathrm{ij}}|n\rangle. \quad (5)$$

In Eq. 5, we have used $\rho = 2330\ \mathrm{kg/m^3}$, while ω_q is obtained from the electron Zeeman energy $E_z = \hbar\omega_q$. The phonon number n_q satisfies the Boltzmann distribution. We choose a temperature range below 100 mK, which guarantees us to be in the low-temperature regime where $(n_q + 1) \sim 1$ [12]. Above 1 K, $(n_q + 1) \sim n_q$, and $1/T_1$ varies as B^4 [20,21]. The polarization vector $\boldsymbol{e_q}$ takes into account the three phonon modes: one longitudinal and two transverse. Since the Zeeman splitting energy is very small (< 1 meV), linear and isotropic bulk Si phonon dispersion is assumed. The phonon wave vector q is then evaluated as $\omega_q = v_s q$, where v_s is the speed of sound in Si, and taken to be 8480 m/s for the longitudinal mode and 5860 m/s for transverse modes. The same constants were also used to interpret the experimental data [12,13]. While local vibrational modes have been observed for P atoms in Si [36], the energy corresponds to the mode frequency is at least an order of magnitude larger than the energy range in interest. The measured T_1 values do not deviate from the B^5 behavior indicates that the local vibrational modes do not contribute significantly to the spin-relaxation process.

Figure 2 shows the spin-lattice relaxation rates, $1/T_1$, of a single P donor and a $4P$ donor cluster as a function of B field. The red squares are the measured rates for a single donor from Ref. [12], whereas the blue triangles are the measured rates for a STM patterned few donor cluster from Ref. [13]. Experimentally, the exact number of donors in the cluster was unknown, but estimated to be between 2 and 5 based on STM images. From transport measurements, it was also expected that during the spin readout step at least three electrons occupied the donor cluster, while in total seven charge transitions on the donor cluster were observed [13].

The red solid line in Fig. 2 represents the calculations performed in this work for a bulk P donor. The calculated rates show a B^5 dependence of $1/T_1$, and also yield similar magnitudes of T_1 (~2.5 s at $B = 2$ T) as the experiment. The B field in this calculation is applied along the [110] direction, consistent with the experiment [12]. To understand the effect of donor number and electron number on T_1, we have simulated donor clusters comprising of two to four donors with various electron occupation. In Fig. 2, we show the results of the $4P$ cluster with one, three, and five bound electrons (the green, cyan, and the blue solid lines, respectively). While the B^5 dependency holds in all cases, the rates vary considerably in magnitude, and increase with the number of electrons. Our calculations show that higher measured relaxation rates of the cluster come from a $5e$ occupation in a $4P$ cluster, which is also consistent with the experimental finding of the electron number being ≥ 3 [13].

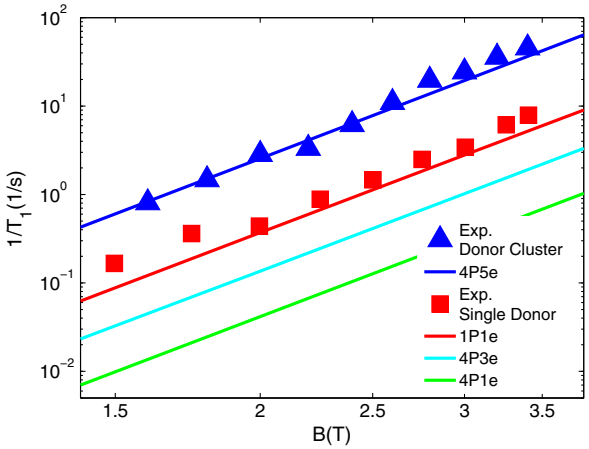

FIG. 2 (color online). Spin-lattice relaxation rates of a single P donor and a $4P$ donor cluster as a function of B field. The red squares and blue triangles show the measured data for a single donor [12] and a few-donor cluster [13], respectively. The solid lines show the TB calculation results for $1P1e$ (red), $4P1e$ (green), $4P3e$ (cyan), and $4P5e$ (blue). $1/T_1$ varies as B^5 for all cases.

We have intentionally chosen an odd number of electrons because the relaxation between a net $1/2$ and $-1/2$ spin is assumed, which requires an unpaired number of electrons. This is also consistent with the experimental measurements, where no spin readout signal was observed for alternate electron occupation in the cluster [13]. The calculations also reveal the startling fact that if we have only one electron in a $4P$ cluster, the relaxation rate is actually smaller than the bulk P, and the T_1 times can be increased from few seconds to hundreds of seconds. The physical reason that determines the magnitude of the T_1 times is also investigated in this work.

To understand the impact of electron number on the T_1 times observed, we determined the electron probability densities of the outermost electrons for varying cluster sizes and electron number in Fig. 3. The size and shape of the wave functions depends on the number of donors and electrons and their locations within the cluster. For the same number of electrons, more donors result in a more tightly bound wave function because of the stronger potential of the larger number of positively charged donor cores. For the

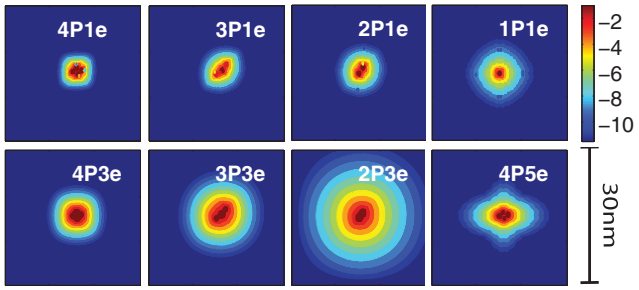

FIG. 3 (color online). The computed probability density (in log scale) of the outermost electron in various donor clusters. The plots show a 2D cut through the center of the clusters.

same number of donors, as more electrons are added, the wave function spreads out more as the donor core becomes more strongly screened. Electron-electron repulsion also causes the wave functions of the outermost electron to spread out more. We have extracted the Bohr radii of these wave functions by fitting an exponential decay function to the tail of probability densities ($|\Psi(r)|^2$) along the x axis through the center of the clusters.

Figure 4(a) shows the relaxation rates (at $B = 2$ T) as a function of the Bohr radii for the same clusters as in Fig. 3. It is observed that donor clusters with larger Bohr radii (i.e., those clusters with more electrons and fewer donors) result in higher relaxation rates. Since the acoustic phonon wavelength corresponding to a Zeeman energy of 0.2 meV (at $B = 2$ T) is about 100 nm, the phonon wavelength is much larger than the electronic wavelengths in this system. A larger electronic wave function therefore interacts with the phonons more [37]. Perhaps more importantly, a larger wave function also implies less quantum confinement in the system, and hence, a smaller energy gap between excited and ground state (i.e., the valley-orbit gap) [38], which relates well to the Hasegawa theory for a bulk donor [20], in which T_1 increases with this energy gap. Since our calculations show a valley-orbit gap ranging from 30 to 5 meV as cluster wave function increases in radii, we expect a strong dependence of T_1 on radii as well. All the calculations presented here also include exchange and correlation effects. We observed that the inclusion of the exchange and correlation effects results in slightly larger wave functions, as the electrons experience greater net repulsion. This causes the relaxation rates to increase slightly and move closer to the experimental data in Fig. 2.

Within a lithographic template for a donor cluster, there can be some uncertainties in the exact locations of the donor [16]. However, if the cluster only comprises of a few donors, all the positional configurations can be enumerated, and the most compact and the most dispersed donor clusters can be identified. Since it is computationally time intensive to simulate all possible donor configurations within a cluster, we have simulated the two extreme cases for donor clusters of one to four donors [Fig. 4(c)]. In Fig. 4(b), we

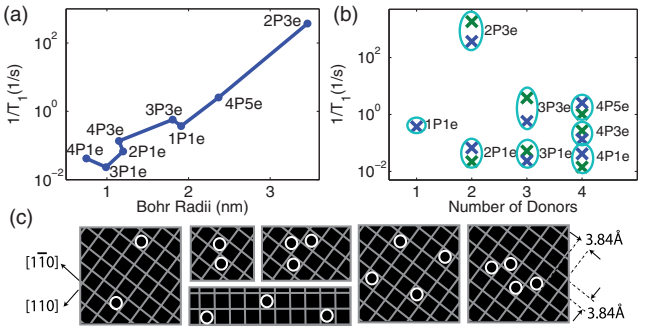

FIG. 4 (color online). (a) The relaxation rates of various donor clusters at $B = 2$ T as a function of the computed Bohr radii of the wave function. (b) The relaxation rates of various donor clusters at $B = 2$ T with different number of electrons. The different points within an ellipse represent the variations in T_1 obtained with different donor locations within the cluster. (c) Exact donor locations for the donor clusters in (b).

have plotted the relaxation rates as a function of electron number for different donor clusters with these two positional configurations (marked by crosses within an ellipse). As expected, the T_1 times have some associated variations with donor locations within a cluster. However, the dependency on the total donor and total electron numbers is stronger. This suggests that T_1 measurements can be used to infer information about donor and electron numbers in STM patterned donor devices, as a noninvasive metrology technique. Such information can be useful for engineering pulses to control single-and two-qubit operations in experiments.

Previous effective mass calculations of Hasegawa [20] and Roth [21] predicted two different spin relaxation mechanisms due to an effective g-factor shift. Hasegawa's mechanism predicts this effective g-factor shift due to the strain induced redistribution of the donor wave function among the six conduction band valleys [20], while Roth's mechanism predicts a single valley g-factor shift due to a strain induced mixing of higher conduction bands [21]. Both mechanisms inherently depend on the spin-orbit interaction in silicon, which reduces the bulk donor g factor slightly below 2. Both Hasegawa and Roth's theory show a B^5 dependency of $1/T_1$ for a bulk donor, but are rather qualitative in nature. The above approaches are also limited to a single bulk donor for which Kohn-Luttinger wave functions can be used [32]. Our TB method captures both mechanisms under the same framework, as a full band structure description is used from the atomic orbital basis including spin-orbit interaction. The method is also general and applies to any nanostructures and semiconductors for which accurate TB models can be developed.

In conclusion, we have presented an atomistic approach to calculate the phonon induced spin lattice relaxation rates in donors in silicon. The T_1 times agree very well with recently measured values on single donors and donor

clusters, and help to explain the variation of T_1 with the numbers of donors and electrons, and the donor locations. The values of T_1 were found to have a strong dependency on the size of the electronic wave functions. This also provides a way to engineer larger T_1 times by using donor clusters with large number of P donors and single electrons. An atomistic description of the T_1 times and their variations in inhomogeneous environment provides crucial information in the design of silicon qubits.

This research was conducted by the Australian Research Council Center of Excellence for Quantum Computation and Communication Technology (Project No. CE110001027), the US National Security Agency and the US Army Research Office under Contract No. W911NF-08-1-0527. Computational resources on nanoHUB.org, funded by the NSF Grant No. EEC-0228390, were used. M. Y. S. received support from a Laureate Fellowship.

*hsuehy@purdue.edu
†rrahman@purdue.edu

[1] A. M. Tyryshkin *et al.*, Nat. Mater. **11**, 143 (2011).
[2] M. Steger, K. Saeedi, M. StegerM. L W. Thewalt, J. J. L. Morton, H. Riemann, N. V. Abrosimov, P. Becker, and H.- J. Pohl, Science **336**, 1280 (2012).
[3] B. E. Kane, , Nature (London) **393**, 133 (1998).
[4] L. C. L. Hollenberg, A. D. Greentree, A. G. Fowler, and C. J. Wellard, Phys. Rev. B **74**, 045311 (2006).
[5] R. deSousa, J. D. Delgado, and S. Das Sarma, Phys. Rev. A **70**, 052304 (2004).
[6] M. J. Calderón, B. Koiller, X. Hu, and S. Das Sarma, Phys. Rev. Lett. **96**, 096802 (2006).
[7] M. Friesen, P. Rugheimer, D. Savage, M. Lagally, Daniel van der Weide, R. Joynt, and M. Eriksson, Phys. Rev. B **67**, 121301 (2003).
[8] C. D. Hill, L. Hollenberg, A. Fowler, C. Wellard, A. Greentree, and H.-S. Goan, Phys. Rev. B **72**, 045350 (2005).
[9] F. A. Zwanenburg, A. S. Dzurak, A. Morello, M. Y. Simmons, L. C. L. Hollenberg, G. Klimeck, S. N. Coppersmith, and M. A. Eriksson, Rev. Mod. Phys. **85**, 961 (2013).
[10] J. J. Pla, K. Y. Tan, J. P. Dehollain, W. H. Lim, J. J. L. Morton, D. N. Jamieson, A. S. Dzurak, and A. Morello, Nature (London) **489**, 541 (2012).
[11] J. J. Pla, K. Y Tan, J. P. Dehollain, W. H. Lim, J. J. L. Morton, F. A. Zwanenburg, D. N. Jamieson, A. S. Dzurak, and A. Morello, Nature (London) **496**, 334 (2013).
[12] A. Morello *et al.*, Nature (London) **467**, 687 (2010).
[13] H. Büch, S. Mahapatra, R. Rahman, A. Morello, and M. Y. Simmons, Nat. Commun. **4**, 2017 (2013).
[14] B. Weber, S. Mahapatra, T. F. WatsonM. Y. Simmons, Nano Lett. **12**, 4001 (2012).
[15] B. Weber, Y. H. M. Tan, S. Mahapatra, T. F. Watson, H. Ryu, R. Rahman, L. C L. Hollenberg, G. Klimeck, and M. Y. Simmons, Nat. Nanotechnol. **9**, 430 (2014).
[16] S. R. Schofield, N. Curson, M. Simmons, F. Rueß, T. Hallam, L. Oberbeck, and R. Clark, Phys. Rev. Lett. **91**, 136104 (2003).
[17] B. Weber *et al.*, Science **335**, 64 (2012).
[18] M. Fuechsle, J. A. Miwa, S. Mahapatra, H. Ryu, S. Lee, O. Warschkow, L. C. L. Hollenberg, G. Klimeck, and M. Y. Simmons, Nat. Nanotechnol. **7**, 242 (2012).
[19] M. Fuechsle, S. Mahapatra, F. A. Zwanenburg, M. Friesen, M. A. Eriksson, and M. Y. Simmons, Nat. Nanotechnol. **5**, 502 (2010).
[20] H. Hasegawa, Phys. Rev. **118**, 1523 (1960).
[21] L. Roth, Massachusetts Institute of Technology Lincoln Laboratory Reports, April 1960 (unpublished).
[22] G. Klimeck *et al.*, IEEE Trans. Electron Devices **54**, 2079 (2007).
[23] G. Klimeck, F. Oyafuso, T. B. Boykin, R. Chris Bowen, and P. von Allmen, Comput. Model. Eng. Sci. **3**, 601 (2002).
[24] J. C. Slater and G. F. Koster, Phys. Rev. **94**, 1498 (1954).
[25] R. Rahman, C. Wellard, F. Bradbury, M. Prada, J. Cole, G. Klimeck, and L. Hollenberg, Phys. Rev. Lett. **99**, 036403 (2007).
[26] S. Ahmed *et al.*, *Springer Encyclopedia of Complexity and Systems Science* (Springer-Verlag GmbH, Heidelberg, 2009), ISBN: 978-0-387-75888-6, p. 5745.
[27] R. Rahman, G. Lansbergen, S. Park, J. Verduijn, G. Klimeck, S. Rogge, and L. Hollenberg, Phys. Rev. B **80**, 165314 (2009).
[28] R. Rahman, S. Park, T. Boykin, G. Klimeck, S. Rogge, and L. Hollenberg, Phys. Rev. B **80**, 155301 (2009).
[29] J. Salfi, J. A. Mol, R. Rahman, G. Klimeck, M. Y. Simmons, L. C. L. Hollenberg, and S. Rogge, Nat. Mater. **13**, 605 (2014).
[30] R. Rahman, G. P. Lansbergen, J. Verduijn, G. C. Tettamanzi, S. H. Park, N. Collaert, S. Biesemans, G. Klimeck, L. C. L. Hollenberg, and S. Rogge, Phys. Rev. B **84**, 115428 (2011).
[31] S. Lee, H. Ryu, H. Campbell, L. C L. Hollenberg, M. Y. Simmons, and G. Klimeck, Phys. Rev. B **84**, 205309 (2011).
[32] W. Kohn, and J. M. Luttinger, Phys. Rev. **98**, 915 (1955).
[33] B. K. Ridley, *Quantum Processes in Semiconductors* (Oxford University Press, New York, 1982).
[34] J. M. Ziman, *Electrons and Phonons* (Oxford University Press, New York, 1960).
[35] T. B. Boykin, G. Klimeck, R. C. Bowen, and F. Oyafuso, Phys. Rev. B **66**, 125207 (2002).
[36] A. S. Barker, Jr., and A. J. Sievers, Rev. Mod. Phys. **47**, S1 (1975).
[37] R. Hanson, J. R. Petta, S. Tarucha, and L. M. K. Vandersypen, Rev. Mod. Phys. **79**, 1217 (2007).
[38] R. Rahman, J. Verduijn, N. Kharche, G. P. Lansbergen, G. Klimeck, L. C. L. Hollenberg, and S. Rogge, Phys. Rev. B **83**, 195323 (2011).